Formation of Solid Methyl Formate and its Isomers in the Interstellar Medium

Mads Mikkelsen
202006293

Bachelor's project
Supervisor: Dr. Sergio Ioppolo

Department of Physics and Astronomy
Aarhus University
Denmark

June 2023

Summary

This Bachelor's project regards the formation of methyl formate and its isomers – molecules with the same molecular formula, but distinct arrangement of atoms – in the interstellar medium. An introduction to the interstellar medium and the surface chemistry happening on interstellar dust grains is provided prior to an experimental section. An astrophysical experiment has been conducted at the ICA facility at Atomki in Debrecen, Hungary, where 1 MeV H^+ ion irradiation on a 20 K pure formaldehyde (H_2CO) deposited on an ice analogue took place. This leads to a description of the facility end station and its relevance to researching astrophysical ice analogues. This project concludes that ion irradiation of H_2CO sparks the formation of carbon monoxide (CO), carbon dioxide (CO_2), methane (CH_4) and methanol (CH_3OH) through its own destruction. This project also provides three different methods for determining the presence of various molecules inside a broad absorption band and discusses the preferred method.

Resumé

Dette bachelorprojekt omhandler formationen af methylformat og dets isomerer – molekyler med samme molekylformel, men forskellig struktur af atomerne – under interstellare forhold. Først gives en introduktion til det interstellare medium og kemien, som finder sted på overfladen af interstellare støvkorn inden det eksperimentelle afsnit gennemgås. Et eksperiment relevant for astrofysik er blevet udført hos ICA i Debrecen, Ungarn, hvor 20 K rent formaldehyde (H_2CO) er blevet bestrålet af 1 MeV H^+ ioner. Dette fører til en introduktion til ICA endestationen og hvordan denne station kan bruges til at forske i astrofysisk is. Dette projekt konkluderer, at ionbestrålingen af H_2CO medfører formationen af kulilte (CO), kuldioxid (CO_2), metan (CH_4) og metanol (CH_3OH) gennem sin egen ødelæggelse. Derudover introducerer dette projekt også tre forskellige metoder for at bestemme tilstedeværelsen af molekyler gemt inde i et bredt absorptionsbånd og diskuterer for den fortrukne metode.

Colophon

Formation of Solid Methyl Formate and its Isomers in the Interstellar Medium.

Bachelor's project by Mads Mikkelsen.

The project is supervised by Dr. Sergio Ioppolo.

Typeset by the author using LaTeX and the memoir document class. Figures are made in Origin Pro together with Python scripts by Guidi Fuchs, Leiden University, NL and Alejandra Traspas Muiña, Queen Mary University of London, UK. Stopping powers calculated by Zuzana Kaňuchová from Slovak Academy of Sciences using SRIM software. Frontpage figure shows the Trifid Nebula (M20, NGC 6514). Image taken by myself and my friend Magnus Ingerslev Uggerhøj using Aarhus University's telescope *FUT* (Fjernstyret UndervisningsTeleskop) located at Mt. Kent, Australia. Image processing done by ourselves in Photoshop.

Contents

Preface

This Bachelor's project delves into the fascinating realm of astrochemistry, specifically focusing on the formation of methyl formate and its isomers. This topic is examined through experiments carried out at the Ice Chamber for Astrophysics-Astrochemistry (ICA) facility located at the Institute for Nuclear Research (Atomki) in Debrecen, Hungary.

I present the destruction and formation rates of formaldehyde (H_2CO), carbon monoxide (CO), carbon dioxide (CO_2), methane (CH_4) and methanol (CH_3OH) along with three different way of determining the abundances of various molecules submerged inside a broad absorption band.

I would like to properly thank all of the people involved in making my trip to Atomki possible and the continuous help and support I have received throughout my project, together with the new friendships I have established along the way.

Concerning my choice of subject, I was intrigued by the mysteries regarding life in space and how this topic is currently researched by some of the frontiers in the field. In this regard, throughout the semester I voluntarily chose to follow an inter-university inter-disciplinary online lecture course called "Astrochemistry: From the Big Bang to Life" hosted by world-leading experts which greatly contributed to my understanding and interest in this field.

1 Introduction

Over the past few decades our notion on the seemingly empty Universe has changed dramatically. The first detection *via* ground-based telescopes of a diatomic molecule, like H_2 and CO, some 100 years ago opened up the doors to the wonders of our molecular Universe [Tielens, 2021]. Recently the field has been accelerating at a great pace due to the availibility of space-based missions such as the Infrared Space Observatory (launched by ESA in 1995), Spitzer Space Telescope (launced by NASA in 2005) [Tielens, 2021] and very recently the James Webb Space Telescope (launced by NASA in 2021) .

Using space-based observations it has become clear that our Universe also consists of, not only simple diatomic molecules, but also complex organic molecules (COMs) comprising of six or more atoms, such as methyl formate, and polycyclic aromatic hydrocarbons (PAHs), an organic compund composed of multiple aromatic rings. Our Universe has a wide variety of chemicals that produces molecules which influence the formation and evolution of stars and galaxies. Studying these molecules can be used to unlock information about the age and properties of areas of interest.

These COMs, including methyl formate and its isomers, are particularly interesting as they are potential prebiotic molecules serving as precursor for molecules like sugars [Simons et al., 2019]. Indeed, a precursor to adenine (one of the four nucleobases of DNA) has been observed in space [Arumainayagam et al., 2019] and plays a vital role in understanding the origin of life.

Firstly, I will give a brief introduction to the interstellar medium and its components and properties before going into the physics and chemistry of dust grains. This brief introduction along with Section (2) will provide a solid foundation for my experimental predictions and further help to understand the results achieved at Atomki.

1.1 The Interstellar Medium

The interstellar medium (ISM) is all of the matter and radiation that exist between the stars in a galaxy and is an ever-changing, dynamical environment [Burton et al., 2013]. In the ISM, matter can either be atomic, ionic, molecular, dust or cosmic rays (CR) and by mass, consisting of ~ 99% gas in any form and

~ 1% is dust particles, or grains, with a size distribution peaking at $r \approx 0.1\mu$m [Herbst, 1995]. The dominant element of matter is hydrogen, followed by helium and then traces of carbon, nitrogen, oxygen and heavier elements [Herbst, 1995] [Linnartz et al., 2015] known as 'metals' in astronomical jargon as these are a result of enrichment due to stellar evolution.

The ISM is by no means homogenous. It varies over many orders of magnitudes in both temperature (T) and density (n). The different components of the interstellar gas are as follows [Ryden and Peterson, 2021]:

- Cold Molecular Cloud (H_2): $T \sim 10\,\mathrm{K}$, $n > 10^9\,\mathrm{m}^{-3}$
- Cold Neutral Medium (H I regions): $T \sim 100\,\mathrm{K}$, $n \sim 10^8\,\mathrm{m}^{-3}$
- Warm Neutral Medium (intercloud medium): $T \sim 7000\,\mathrm{K}$, $n \sim 4{\times}10^5\,\mathrm{m}^{-3}$
- Warm Ionized Medium (H II regions): $T \sim 10^4\,\mathrm{K}$, $n \sim 10^6\,\mathrm{m}^{-3}$
- Hot Ionized Medium (coronal gas): $T \sim 10^6\,\mathrm{K}$, $n < 10^4\,\mathrm{m}^{-3}$

Each of these components of the ISM have very different properties. Although the coronal gas comprises ≥ 50% of the *volume* of the ISM, it only accounts for a tiny fraction of the *mass*. Whereas the cold molecular clouds comprise ~ 30% of the *mass* whilst only occupying ~ 0.05% of the *volume* [Ryden and Peterson, 2021].

Naturally, there are also different ways to detect the interstellar gas depending on which component one is examining. The first method is mm-wavelength **radio line emission**, which is the characteristic property for the denser regions of the ISM (in cold molecular clouds), where individual molecules can join together and form molecules such as CH and CO amongst the most common. For instance, when a CO molecule transitions from a rotational state $J = 1$ to $J = 0$, it emits a photon with $\lambda = 2.6\,\mathrm{mm}$, where Earth's atmosphere happens to be transparent. Then the interstellar gas can also be detected when neutral hydrogen (H I) radiates line emission in the **21-cm wavelengths** *via* the hyperfine atomic transitions in the ground state, where the main tracers are UV and optical absorption lines [Osterbrock, 1984].

Another method of gas detection is when an object, like an emission nebula such as the Trifid Nebula on the front page, produces an **emission spectrum**. These spectra occur after electrons get excited from their ground state by absorption of a photon and eventually recombine and emit a photon related to the energy levels jumped. Ultimately, interstellar gas can be detected when it creates **absorption lines** in a star's spectrum. Its main tracers are absorption lines in the far-UV (e.g., O IV, N V and C IV) in gas with $T \sim 10^5$ K, and soft X-ray emission from gas hotter than $T \sim 10^6$ K.

1.2 Dust Grains and Surface Chemistry

Around 1784, William Herschel, the German-born British astronomer and composer, discovered a patch in the night sky where there appeared to be an absence of stars. Herschel called these apparent voids for "holes in the sky" and this was probably the first evidence that there existed material in space between stars – the interstellar medium – that was capable to absorb and scatter the emitted starlight. It is now known that this material was small interstellar dust grains [Williams and Herbst, 2002].

Interstellar dust grains are tiny solid particles that exist in the ISM. The composition of these dust grains are mainly considered to be either silicates or consisting of carbonaceous material [Tielens, 2021], but other less abundant materials could also be present. The grains can range in size from a few molecules to micrometers. Although interstellar dust only makes up about ~ 1% of the total mass of the ISM, it plays a crucial role in shaping the physical and chemical properties of the regions between stars. Interstellar grains absorb and scatter light, affecting the appearance and color of starlight making observational astronomy even more difficult. Additionally, dust grains provide a surface on which species can accrete, meet and react – prompting complex chemistry.

The parameters setting the boundaries for reactions on grains are the accretion rate – which sets the time scale for the process – and the surface migration rate – which controls the reaction network [Tielens, 2021]. When a gas phase species, for instance atomic H, approaches a surface from a large distance, it will feel a weak attraction due to the van der Waals force. As the distance decreases, this leads to stronger bindings and eventually sticking due to shared electrons. These two types of interactions can be recognized as the *physiosorbed site* due to van der Waals interaction and the *chemisorbed site* in the case of shared electrons.

2 Theory

In the following section, I will describe the characteristics of surface chemistry where I will introduce different models for ways atoms can accrete and react on interstellar dust grains. Hereafter, I will explain the underlying theory of infrared spectroscopy and provide a theoretical background for the experimental components introduced in Section (3) and some of the techniques that are useful in regards to performing experiments. Lastly, I will describe what happens when an interstellar dust grain gets irradiated by high energy ions and what this process can be related to.

2.1 Chemistry on Interstellar Grain Surfaces

The chemistry that occurs in the ISM is typically very different than that we experience on Earth due to the harsh environment in outer space. Molecular formation is generally thought to happen mainly in dense molecular clouds, as the interiors of such clouds are shielded from far- and vacuum-UV radiation and are characterized by the low temperatures (10 – 20 K) and high particle number density (10^2 – 10^6 cm^{-3}) [Herczku et al., 2021].

Under these conditions, atoms and molecules such as H, H_2, O, C, N, CO, NO *et cetera* freeze out onto the interstellar dust grains. Molecules entrapped in the icy mantle of dust grains can be a part of interesting chemistry induced by some form of energetic processing, *e.g.* X-rays or CR, both of which are able to penetrate the dense molecular cloud [Herczku et al., 2021].

Gas phase species can collide with the interstellar grains and stick in physiosorbed sites. From here the atoms can either transfer to a chemisorbed site or they can desorb and leave the grain again. Species with low barriers, *e.g.* atomic hydrogen, will be mobile and migrate the icy grain searching for reaction partners. This process is called the *Langmuir-Hinshelwood* process and is one of the main processes for chemical reactions on interstellar grain surfaces. Besides the Langmuir-Hinshelwood, gaseous species may interact with a trapped and immobile species on the ice grain and promt a reaction - this process is called the *Eley-Rideal* process. The last main process happening on the surface of interstellar grains is the *Harris-Kasemo*, or *Hot-Atom* process, where an accreting species may come in and during thermal acclimation

migrate and find a reaction partner [Tielens, 2021]. These three processes are illustrated in Figure (2.1).

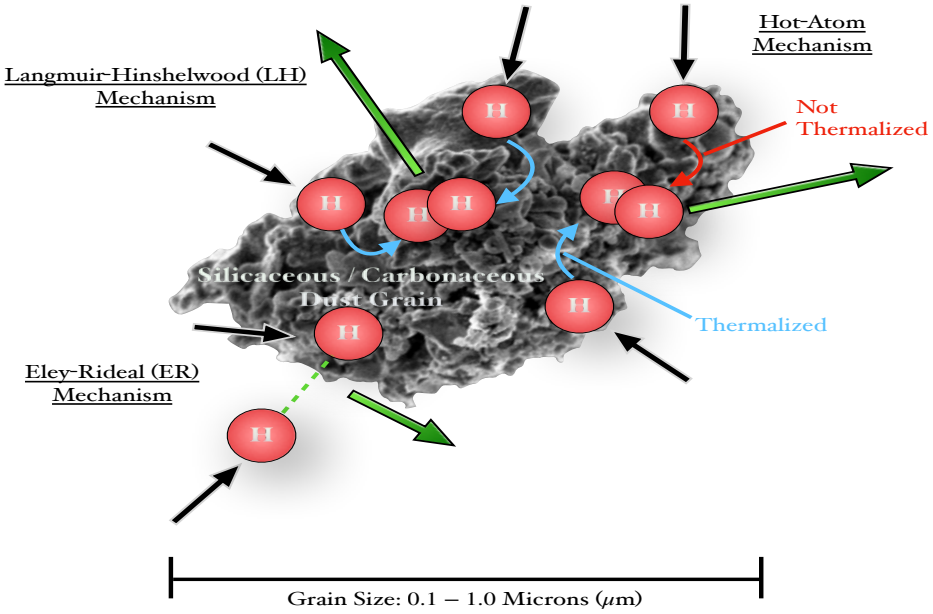

Figure 2.1: Illustration of the three main characteristic processes of surface chemistry on bare dust grains. Image inspired and adapted from [Arumainayagam et al., 2019] using image of dust grain by [Michael Richmond from http://spiff.rit.edu/classes/phys230/lectures/ism_dust/ism_dust.html].

Over long periods of time material will continue to accumulate and eventually lead to the formation of a nanoscale ice mantles consisting of H_2O, CO_2, CO, CH_3OH, NH_3, and CH_4 [Arumainayagam et al., 2019]. These ice layers allow for interstellar ice processing – either non-energetically (thermal chemistry and atom addition chemistry) and energitcally (shock chemistry, photochemistry and radiation chemistry) – where a couple of them will be discussed in the following section – which can lead to the formation of COMs and other interesting chemistry.

COMs, *e.g.* formaldehyde, are thought of to result from grain surface reactions through the following hydrogenation reaction

$$\mathrm{CO} \xrightarrow{\mathrm{H}} \mathrm{HCO\bullet} \xrightarrow{\mathrm{H}} \underset{\text{Formaldehyde}}{\mathrm{H_2CO}} \,, \tag{2.1}$$

however through energetic processes (*i.e* CR irradiation) the bonds can break and reverse the process leading to radical-radical recombination

$$\mathrm{H_2CO} \xrightarrow{\mathrm{CR}} \mathrm{HCO\bullet + H} \xrightarrow{\mathrm{O}} \mathrm{HCOO\bullet} \xrightarrow{\mathrm{C}} \underset{\text{Formic Acid}}{\mathrm{HCOOC}} \xrightarrow{\mathrm{3H}} \underset{\text{Methyl Formate}}{\mathrm{HCOOCH_3}} \,. \tag{2.2}$$

All of these COMs (*e.g.* methyl formate, glycolaldehyde, ethelyne glycol) have been observed in dark molecular clouds, however since a gas phase route to produce these species is not efficient [Tielens, 2021] [Simons et al., 2019] it is suspected to happen on top of low temperature dust grains [Bacmann et al., 2012][Simons et al., 2019].

Ice Deposition

As mentioned previously, the first ice layer consists of H_2O and CO_2, however as time progresses and the cloud that the dust grains exist within evolves, the density will increase leading to heavier molecules condensating onto the dust grains to form a second ice layer. As the inner-most ice layer is predominantly H_2O the resultant molecular ice is polar in nature [Whittet et al., 2013] whereas the second layer will be non-polar due to most of the gas condensating being CO [Pontoppidan, 2006].

Icy grain mantles are thought to be the main reservoir from which COMs in the ISM originate from, as gas-phase chemistry is thought to be insufficient to account for the observed abundances of these species [Herbst and van Dishoeck, 2009][Arumainayagam et al., 2019]. The molecular formation in astrophysical ices is driven by five mechanism – either energitically or non-energitically, introduced in the previous section. Although all of the processes are relevant for the processing of interstellar dust grains, given the scope of this project, I will constraint myself to introducing only the most relevant processes – atom addition and radiation chemistry.

Atom addition reactions have already been invoked in understanding the formation of the polar layer on interstellar icy grain mantles, such as the formation of H_2O through hydrogenation or formation on the surface of the ice yielding formaldehyde *via* Equation (2.1). Atom addition reactions can form simple molecules such as CO_2 through the reaction of CO with an -OH radical [Ioppolo et al., 2011] and through an advanced network of atom or radical addition reactions create complex molecules such as CH_3CH_2OH or NH_2CH_2COOH [Ioppolo et al., 2021].

Astrophysical ices are often found in environments that are bombarded by energetic charged particles (*e.g.* ions and electrons) driven by galactic cosmic rays, stellar winds *et cetera* [Duncan V. Mifsud, PhD Thesis 2023]. These processes can cause a change in the morphology (*i.e.* the structure – whether it being crystalline or amorphous) *via* ice sputtering, compaction of structure and more [Duncan V. Mifsud, PhD Thesis 2023]. Many of the astrophysical radiation environments are characterized by particles having energies in the range of a few keV to a few MeV [Arumainayagam et al., 2019].

Usually, the detection of gas-phase interstellar molecules are achieved *via* rotational spectroscopy, however, given the solid state of interstellar ices which excludes the possibility of rotational vibrations, other methods have to be taken in use. One of these methods is called infrared spectroscopy and will be discussed in the following section.

2.2 Spectroscopy

Spectroscopy is the field of study that measures and interprets an electromagnetic spectrum acquired by the interaction between electromagnetic radiation and matter. From the acquired spectrum, valuable information concerning the structure and properties of matter can be unveiled. Spectroscopy builds on the theory that light is made of different wavelengths and therefore different frequencies related by the following equation

$$c = \lambda \nu, \tag{2.3}$$

where c is the speed of light in vacuum, λ is the wavelength and ν is the frequency. Light consists of photons with quantised packets of energy (E) directly correlated to the frequency through the following

$$E = h\nu, \tag{2.4}$$

where h is the Planck constant. There exists many sub-disciplines of spectroscopy depending on the type of energy involved and the interaction between the energy and the material – *e.g.* emission spectroscopy, molecular spectroscopy and infrared spectroscopy to name a few. Spectroscopy is an incredibly powerful tool for astronomers as it allows for observations of specific energies associated with molecular rotation and vibration unique to a certain molecule of interest. Rotational transitions arise from the rotation of a permanent dipole interacting with an oscillating electromagnetic field, whilst a vibrating molecule undergoes a change in dipole moment and couples to an electromagnetic field [Tielens, 2021]. Vibrational spectra of molecules frozen into an ice differs in many ways from that of a gas phase spectra. Solid state molecules tend to have rotations suppressed thus collapsing the rotational-vibration band to one absorption band near its band origin. However, this band position will also differ from that of the free, gas phase molecule due to repulsive interactions *et cetera* with neighboring molecules. This causes a shift in the observed band up to hundreds of wavenumbers [Tielens, 2021].

Applicable to all of the different sub-disciplines of spectroscopy is their relation to the electromagnetic spectrum. Where ultraviolet (UV) spectroscopy

provides information on the transitions of the valence (or outer shell) electrons, IR spectroscopy will provide information on the molecular vibrational transitions [Rachel J. James, PhD Thesis 2019]. Usually, UV spectroscopy is quoted in units of electronvolts (eV). Whereas, the most commonly used unit for IR spectroscopy is the reciprocal of wavelength - the *wavenumber* (cm^{-1})

$$\tilde{\nu} = \frac{1}{\lambda}. \tag{2.5}$$

The following section will be a further description of IR spectroscopy as it holds many astrophysical applications.

Infrared Spectroscopy

Infrared spectroscopy – also called vibrational spectroscopy – is a technique used to identify and analyze chemical substances based on their absorption of infrared radiation with matter.

IR spectroscopy allows for the identification of functional groups which are a specific group of atoms within a molecule that determines its chemical properties and reactivity. Includes, but not limited to, the hydroxyl group (-OH), carbonyl group (C=O), carboxyl group (-COOH) and the aldehyde group (-CHO), all of which appear throughout this project.

The IR portion is usually divided into three regions: the near-, mid- and far- infrared (NIR, MIR and FIR, respectively), named for their relation to the visible spectrum [Alejandra T. Muiña, PhD thesis, In preparation]. An IR spectrum is simply the plot of IR radiation versus the wavelength (or equivalently, the wavenumber).

A common laboratory instrument that uses IR spectroscopy is a Fourier-Transform Infrared Spectrometer that allows for identification of chemical bonds in a molecule. As Fourier-Transform Infrared Spectroscopy plays a vital role in the study of astrophysical ice analogues and being the method I have used at the Ice Chamber for Astrophysics-Astrochemistry facility in Hungary, I have dedicated an introduction within Section (3.3) to Fourier-Transform Infrared Spectroscopy at the facility.

2.3 Ion Irradiation

Ions striking ice will produce a number of effects due to elastic and inelastic collisions with the target molecules, and consequent loss in ion energy. The important effects of ion irradiation on ices involves **sputtering** – resulting in a loss of material and ejection of atoms or molecules into gas phase – and **change in physical properties of the ice** – *e.g.* amorphisation (the change

of phase from ordered crystalline structure to a random amorphous structure) of ice [Anita Dawes, PhD Thesis 2003].

In an astrophysical environment, these effects amongst others will happen simultaneously. The extent of these effects are controlled by the properties of the ice (composition, temperature and thickness) and the ions (energy, flux and type). In interstellar space, these processes can be attributed to CR consisting of high-energy ions as cosmic rays can penetrate the shielding near molecular clouds and protoplanetary disks.

3 Experimental Setup

As a part of my Bachelor's project, I had the chance to investigate astrochemistry at first-hand as I got the chance to travel to the Institute for Nuclear Research (Atomki) in Debrecen, Hungary and experience the Ice Chamber for Astrophysics-Astrochemistry (ICA) facility and participate in some experiments.

In this section, I wish to account for all of the different components present at the ICA facility end station and why the components are necessary for the experiment. Subsequently, I will express some experimental considerations and concepts for data collection. Following that section, I will go through the experimental methodology and describe how to prepare a sample, depositing molecules, resolutions *et cetera*. This section builds upon the theory established in Section (2) and provides a framework for the results presented in Section (4) and discussed in Section (5).

3.1 Introduction to the Components at the Facility

The facility end station is an ultra-high vacuum (UHV) chamber capable of being cooled down to 20 K *via* a closed-cycle helium cryostat to simulate interstellar conditions [Mifsud et al., 2021] [Herczku et al., 2021]. The experimental setup begins with a 2 MV tandetron accelerator passing ions through a collimating slit consisting of two sets of 4x4 electrode steerer plates, one vibrating perpendicular and one parallel to the beam at a low frequency and a high frequency respectively. This allows for scanning of a square (similar to an old TV screen) resulting in very precise measurements of the middle position of the beam. Afterwards the beam is sent through another collimator and a quartz. The quartz is another indicator of the homogenity of the beam as a completely homogeneous beam will produce a desired circular output. The beam then travels through a series of Faraday cups measuring the current throughout the setup. The first two Faraday cups measures a ratio before the beam enters the sample and the final Faraday cup is placed at the far end of the setup. It is designed in such a way that the final Faraday cup measures

exactly half of the first input. This ensures that the published values for the fluence is the correct value and not just a theoretically calculated fluence.

The UHV compatible chamber comprises 10 CF40 (conflat flange of size 40) ports allowing for additional external modules to be introduced into the setup. Each of which are separated by exactly 36° from one another. In the center of the chamber is a an infrared (IR)-transparent sample holder allowing for up to four substrates where interstellar ice analogues – in our case zinc selenide (ZnSe) – can be deposited to be examined under identical conditions [Mifsud et al., 2021]. The sample holder is equipped with a thermometer at the top and the bottom of the holder to identify any eventual temperature gradient that might affect the measurements. The entire holder and cryostat is able to rotate so that the sample can always face the desired CF40 port connected to a specific module.

To the right of the beam line is the first module – the IR beam module, allowing for IR spectroscopy measurements. Next to the IR beam module is the Kimball ELG-2A electron gun able to emit electrons in the 5 – 2000 eV range [Mifsud et al., 2021]. Directly opposite of the electron gun is another Faraday cup allowing for measurements of the beam's stability and intensity. Additionally, this port also contains a deposition line directly in line with the substrate in the middle of the chamber. Next to the electron gun is the quadrupole mass spectrometer (QMS) which separates molecules depending on their charge.

Continueing 36° around, we encounter the background dosing line – this module allows for mixing of chemicals that will be deposited onto a distributor (scattering) plate behind the sample. Since CO, CO_2, CH_4 etc. are all gasses, they require a two valve system to ensure correct pressure and flow, but H_2O and diethyl ether are liquids and therefore do not need a two valve system. The valves also ensure known volumes and a constant flow of deposition *via* a constant pressure. When the mixture gets deposited from the back, it will hit a distribution plate causing the gas to spread in a very homogeneous way and stick to the substrate homogeneously. At the very end of the setup is the last Faraday cup mentioned earlier. Next to the Faraday cup is the mercury-cadmium-telluride (MCT) detector which is a very efficient IR detector.

Next to the MCT detector, directly opposite of the electron gun, is another Faraday cup combined with a deposition line. This deposition line carries a moveable deposition needle that allows for direct exposure onto the substrate. This is very ideal for depositing formaldehyde, which is a powder at room temperature. The last two ports are a vacuum gauge and an optical viewport, respectively. It is important to notice, that the pressure gauge cannot go from atmospheric pressure to UHV but needs to go through an intermediate

vacuum step – the so-called "UHV Prevac". A schematic overview of each of the components can be seen on Figure (3.1). See Appendix E for pictures taken at the ICA facility along with some pictures of the components.

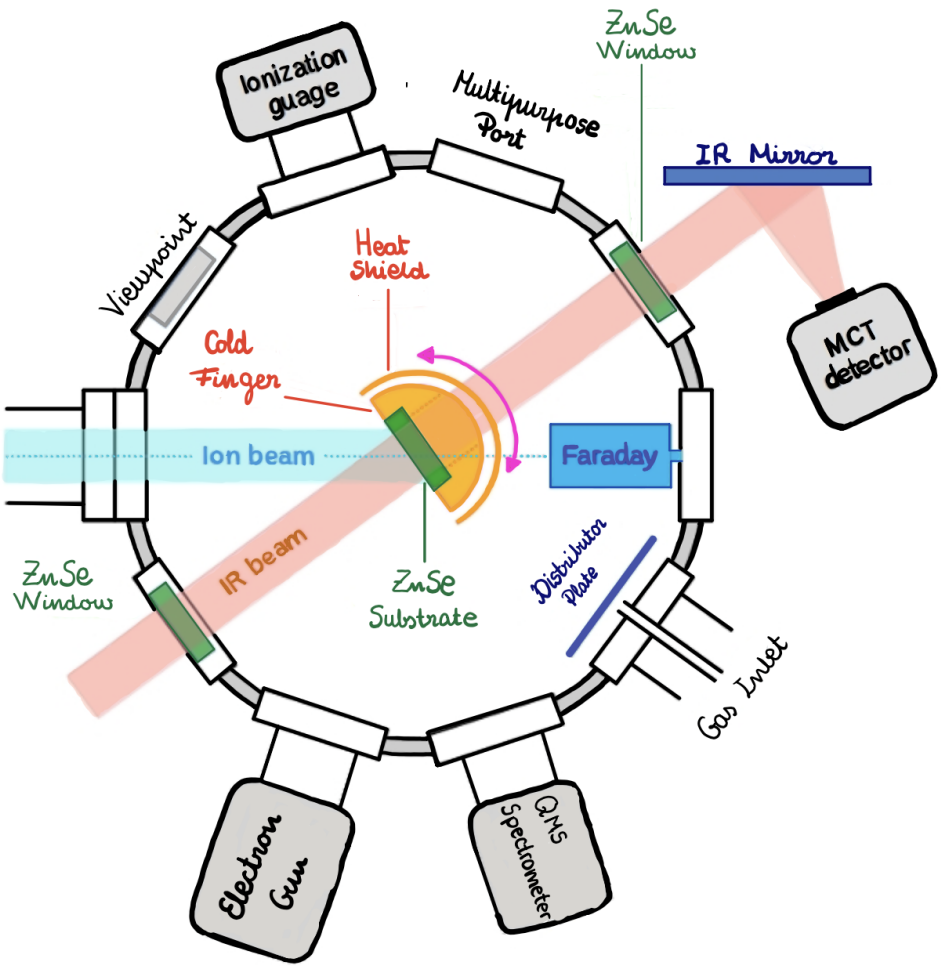

Figure 3.1: A schematic overview of the ICA end-station at Atomki. Each of the modules are introduced and described in the beginning of Section (3), but consists of 10 modules each separated by exactly 36°. Although the sample holder is rotatable it is depicted as being perpendicular to the IR beam as when collecing a spectrum. Image obtained from [Alejandra T. Muiña PhD Thesis, in preperation].

3.2 Experimental Consideration and Measurement Concepts

Several considerations have to be made regarding the thickness of our ice analogue. Since we want to replicate interstellar conditions we will need thicknesses that accurately represent interstellar dust grains and the environments they exist in.

Ice Thickness

Since we were interested in examining the effect of CR we wanted a thin layer of ice to prevent CR implantation and make sure the CRs penetrate right through. To estimate this, we need knowledge on the rate of energy loss (*i.e.,* the stopping power, Equation (4.2)) of the projectile charged particle. However, it is incorrect to assume that the stopping power is constant throughout the target medium. Indeed, plots of stopping power acquired from [Zuzana Kaňuchová, Slovak Academy of Sciences] – see Appendix A – demonstrate that the maximum loss of energy (the so-called Bragg peak) occurs just before it comes to rest within the target medium.

Temperature

In addition to the ice thickness, the temperatures must also represent the inhospitable interstellar conditions with low temperatures and near zero pressures [Arumainayagam et al., 2019]. Since we are interested in examining the formation of methyl formate and its isomers in the interstellar medium, we will have to recreate similar conditions for these COMs to form. From Section (1) this is found to be within dense molecular clouds and *via* grain surface reactions through Equation (2.2). Therefore, the ICA facility proves very useful for simulating interstellar conditions as we can reach temperatures as low as 20 K for dense molecular clouds relevancy.

Energy

One of the major advantages of the ICA facility is its connection to the tandetron beamline. This allows for mid- to high energy ion irradiations of astrophysical ice analogues. Since CR are among the only forms of radiation that can penetrate the shielding in dense molecular clouds, we carried out our experiments with 1 MeV H^+ to simulate the effect of CR.

3.3 Experimental Methodology

Before starting the collection of a spectrum, we have to calculate the targeted fluence. This is done by irradiating our sample with a given ion flux then by integrating over a time period will give us the fluence. The beam current, which can be used to derive ion fluxes, is measured by the Faraday cups introduced in Section (3.1). During an experiment we take two measurements: firstly, we calculate the ratio between the two Faraday cup measurements, then by knowing this ratio and irradiating at a given energy (1 MeV in this case) for a specific time period (100 seconds) we can calculate the fluence (Φ) quite easily using

$$\Phi = \frac{\Delta Q_{\text{Total}} \times 10^{-6}}{nqA_{\text{Irradiated}}}, \tag{3.1}$$

where n is the charge state of the incident ion and the factor 1×10^{-6} changes from μC to C, $A_{\text{Irradiated}}$ is the irradiated area.

However, one important thing to notice is we have to take the incident angle between the H^+ beam and the substrate into consideration as this makes the beam appear as an elongated circle (elipsoidal) instead of a uniform circle as seen from the sample. This introduces a sort of "form factor" into the intensity equation, which is where the factor of 0.734 comes from.

$$\Delta Q_{\text{Total}} = \sum \Delta Q_{\text{FC1}} \times \left(\frac{\Delta Q_{\text{FC1}}}{\Delta Q_{\text{FC2}}} \right) \times 0.734, \tag{3.2}$$

with ΔQ_{FC1} and ΔQ_{FC2} being the electric charge for Faraday cup 1 and 2, respectively. The measured dimensionless ratio between ΔQ_{FC1} and ΔQ_{FC2} ensures the measured charge is proportional to the incident current.

The sample is prepared by first annealing it, which means heating it up to a high temperature to dissolve any unwanted substances or contaminations in the chamber. Then the sample is gradually cooled to 20 K, which is the limit using the facility at Atomki, however this also accurately resembles the necessary astrophysical conditions in molecular clouds described in Section (1.1). Then we had to heat up the H_2CO as it is a powder and we wanted to deposit it *via* the all-metal needle valve placed a few millimeters from the ZnSe substrate (using "Multipurpose Port" in Figure (3.1)).

The pressure inside the vacuum chamber reached 5×10^{-9} mbar (UHV) before depositing, but during deposition the presure naturally rises as we introduce a substance into UHV. The pressure reached 1×10^{-6} mbar during deposition and slowly decreased afterwards. The deposition could be followed *in situ* using a technique called Fourier-Transform Infrared Spectroscopy (FTIR) which will introduced further in the following section.

Fourier-Transform Infrared Spectroscopy (FTIR)

FTIR obtains a high resolutions IR absorbance spectrum over a broad spectral range. The spectral range at Atomki is 4000 – 650 cm^{-1} with a resolution of 1 cm^{-1} [Mifsud et al., 2022]. Using this, a quantitative measurement of the ices' column densities N (molecules cm^{-2}) and thickness d (μm) could be performed by measuring the peak area P (cm^{-1}) of a characteristic absorption band using a combination of Equation (3.3) and (3.4) [Mifsud et al., 2022]

$$N = \frac{P \ln(10)}{A_\nu}, \tag{3.3}$$

$$d = 10^4 \times \frac{NZ}{N_A \rho} = 10^4 \times \frac{PZ \ln(10)}{N_A A_\nu \rho}, \tag{3.4}$$

where A_ν is the integrated absorption band strength for the band (cm $molecule^{-1}$), Z is the molar mass of deposited ice (g mol^{-1}), N_A is the Avogadro constant (6.02×10^{23} molecules mol^{-1}) and ρ being the mass density of the ice (g cm^{-3}).

Knowing the thickness of the deposited ice we can use software (such as SRIM [Ziegler et al., 2010]) to make sure ions are passing through our sample and not implanted within.

Quadrupole Mass Spectrometer (QMS)

The ICA facility is also equipped with a quadrupole mass spectrometer (QMS) that allows for a qualitative monitoring of the gas-phase composition of the main chamber. A QMS consists of four parallel metal rods, each opposing rod being electrically connected together. Only ions with a certain mass-to-charge ratio will be able to travel through the rods and reach the detector. Other ions with unstable trajectories will collide with the rods. This is mostly relevant during ion irradiation and thermal annealing, wherein molecules may sputter or desorb, respecively, from the ice.

The QMS presently attached to the ICA facility allows for detections of sputtering or desorption of molecules with a molecular mass of up to 200 amu at a mass resolution of 1 amu [Duncan V. Mifsud, PhD Thesis 2023].

4 Results

4.1 Deposition vs. Irradiation

The FTIR spectra of pure H_2CO ice, both before (solid black line) and after irradiation of 1 MeV H^+ ions at a dose of 11 eV/16u at 20 K (solid red line), are depicted in figure (4.1).

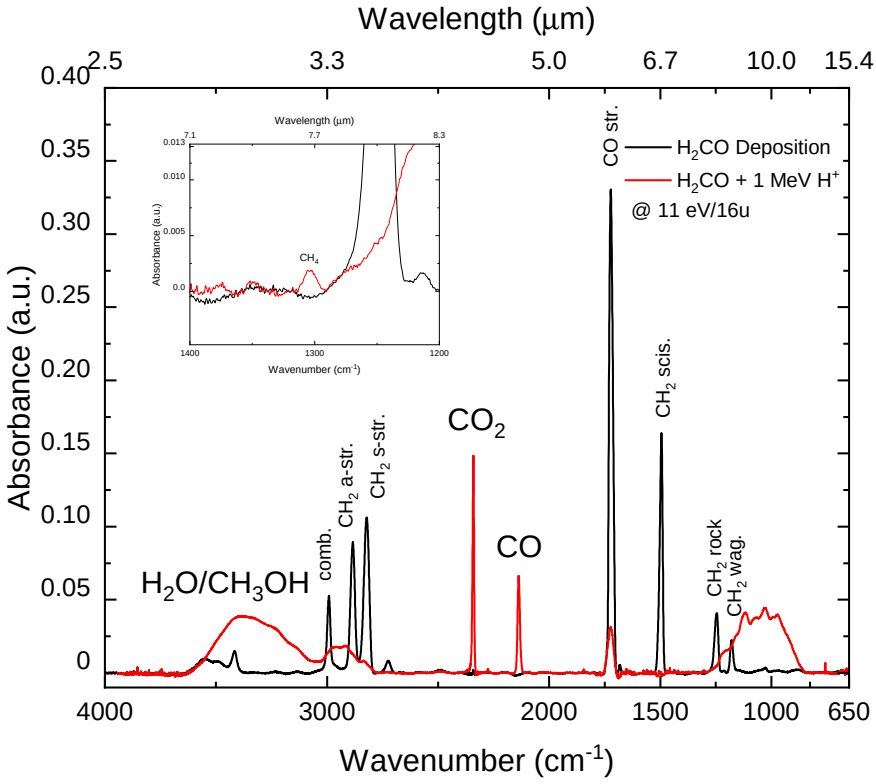

Figure 4.1: FTIR spectrum of pure H_2CO deposition (solid black line) together with FTIR spectrum of the ice irradiated by 1 MeV energetic ions at 20 K (solid red line). Additionally, each of the characteristic modes for H_2CO have been labeled together with the absorption peaks for CO, CO_2 and CH_4 which are also the absorption bands used to calculate the area used in the calculation for column densities. Moreover, the characteristic broad band for water and methanol (CH_3OH) is also labeled. See Appendix B for enlarged figure.

4.2 Column Density & Band Strength

To examine the formation or destruction of various species and to be able to compare them, it is necessary to take into account the different properties for each of the molecules. Each species have different band strengths and areas which will effect the column density in the following way

$$\mathrm{CD} = \frac{\ln(10) \times \mathrm{Area}}{\mathrm{Band\ Strength}}, \tag{4.1}$$

where CD is the column density, the area is found by using the python script from [Guidi Fuchs, Leiden University] to integrate under each of the molecule-specific prominent peaks for each of the irradiations and the band strengths are found in [Bouilloud et al., 2015] and also listed in Table (4.1) for each of the species examined.

The dose is calculated *via* Equation (4.2) where the retarding force acting on a particle as it passes through a material – the *stopping power* – and loses some of its energy is taking into account

$$\mathrm{Dose} = \mathrm{Fluence} \times \mathrm{Stopping\ Power}, \tag{4.2}$$

where the fluence is experimentally achieved *in situ* and the stopping power has been simulated by [Zuzana Kaňuchová, Slovak Academy of Sciences] using software from [Ziegler et al., 2010] called SRIM - the Stopping and Range of Ions in Matter. The stopping power is found to be $7.82 \times 10^{-15}\ \frac{\mathrm{eVcm}^2}{16\mathrm{u}}$ thanks to Zuzana.

Species	**Absorption Band Position** $\left[\mathrm{cm}^{-1}\right]$	**Band Strength** $\left[\frac{\mathrm{cm}}{\mathrm{molecule}}\right]$
H_2CO	1500	5.1×10^{-18}
CO	2139	1.12×10^{-17}
CO_2	2343	7.6×10^{-17}
CH_4	1302	8.0×10^{-18}

Table 4.1: Some of the physical parameters used for the calculations of column density for the species formaldehyde (H_2CO), carbon monoxide (CO), carbon dioxide (CO_2) and methane (CH_4). Literature values for the band strengths are found from [Bouilloud et al., 2015].

4.3 Destruction and Formation

Figure (4.2a) depicts the destruction of formaldehyde (H_2CO) due to irradiation of 1 MeV H^+ ions at 20 K. Figure (4.2b) shows the formation of carbon monoxide (CO) through the 1 MeV H^+ ion irradiation of formaldehyde at 20 K. Figure (4.2c) shows the formation of carbon dioxide (CO_2) through the 1 MeV H^+ ion irradiation at 20 K. Figure (4.2d) depicts the formation of methane (CH_4) when formaldehyde is irradiated with 1 MeV H^+ ions at 20 K. Lastly, Figure (4.2e) shows the formation of methanol (CH_3OH) after H_2CO gets irradiated with 1 MeV H^+ ions at 20 K. Areas are acquired by gaussian fitting of peak 7 in Figure (4.3b) or (4.3d) which lies directly within the broad band. Therefore, a significant uncertainty follows the column density, however the general behavioral trend is trustworthy.

4.4 Determination of Broad Band

Figure (4.3a) shows the labelling of all of the different pure ice components that could make up the observed spectrum of H_2CO irradiated with 1 MeV H^+ ions at 20 K at the dose 11 eV/16u. The pure ice spectra have been scaled and spaced apart to allow for better identification and determination of the central band position and therefore do not represent abundances. Figure (4.3b) shows one way of determining what the peaks in the broad band could consist of using a linear way of integration beneath the peaks. However, this way has some serious downsides as discussed in Section (5). Figure (4.3c) shows another way to determine the contributions of the individual pure ice species by adding each of the spectra to create a fit this way. The disadvantages of this method are discussed in Section (5). Lastly, Figure (4.3d) shows the preferred way of disentangling a broad band. It is done by fitting a gaussian underneath each peak and then calculate the area in this region throughout each irradiation. This method is further discussed in Section (5).

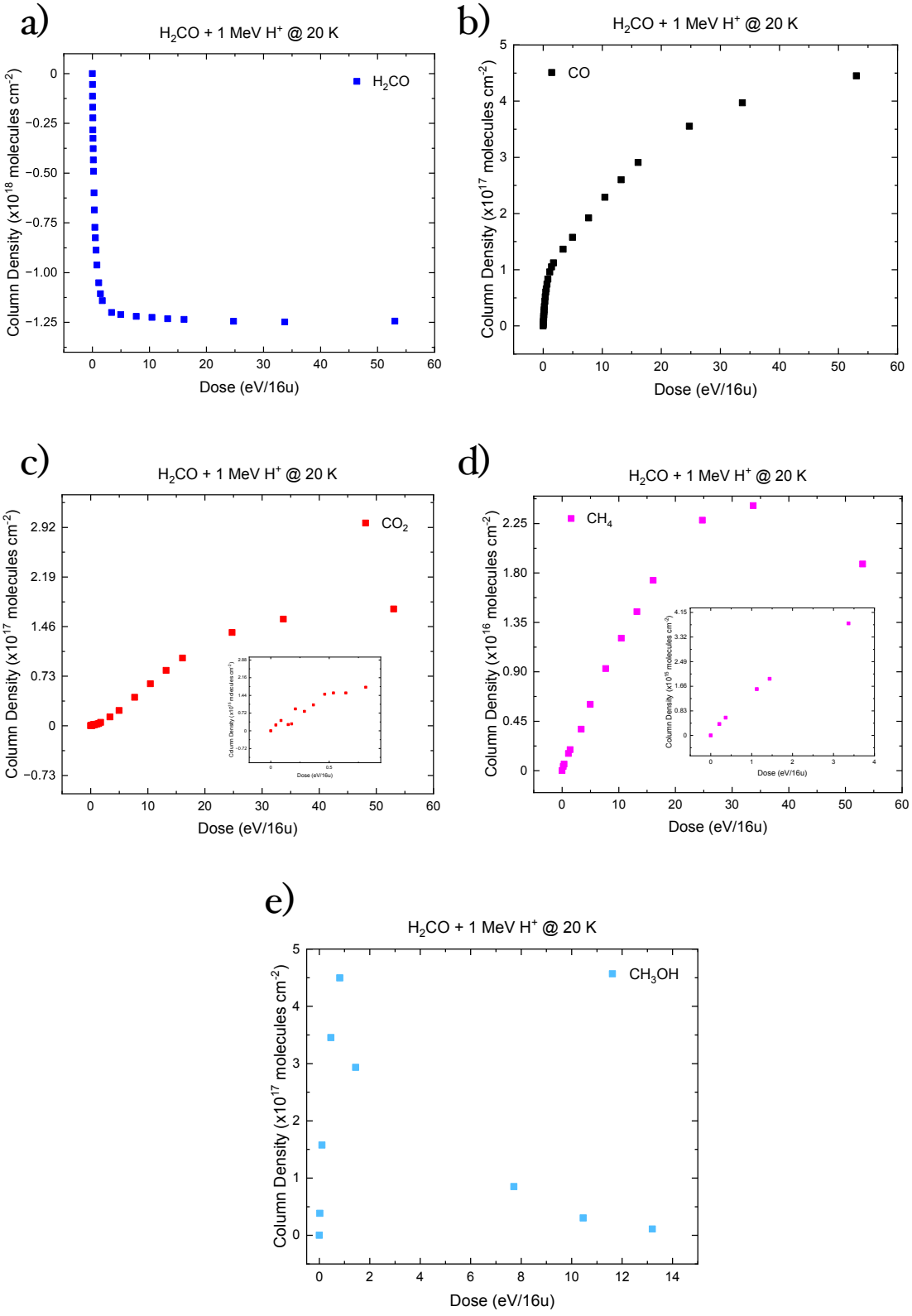

Figure 4.2: Figures showing the formation of **b)** CO, **c)** CO_2, **d)** CH_4, **e)** CH_3OH when **a)** H_2CO gets irradiated by 1 MeV H^+ ions at 20 K. See Appendix C for enlarged individual figures.

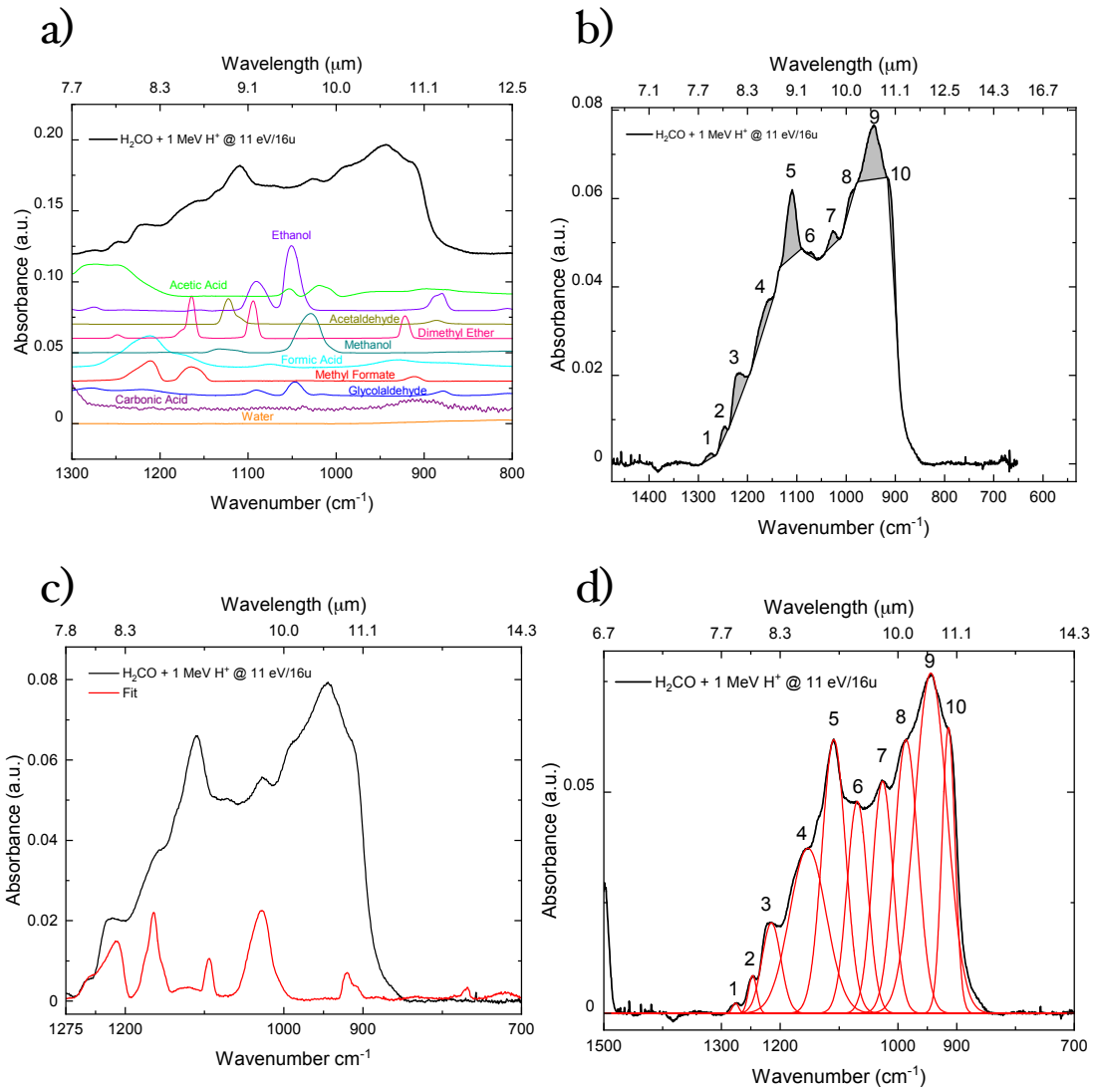

Figure 4.3: Three different methods to determine the components of the broad band spectrum of pure H_2CO irradiated with 1 MeV H^+ ions at 20 K at the dose 11 eV/16u. **a)** shows the different pure ice components scaled and labeled where their individual contributions have been added together to make the fit in **c)**. **b)** shows the linear fitting method and **d)** shows the preferred gaussian fitting. See Appendix D for enlarged individual figures.

5 Discussion

I was able to be a part of performing multiple laboratory experiments at Atomki in Debrecen, Hungary. In particular we analyzed a sample of pure formaldehyde (H_2CO), a mixture of formaldehyde and carbon monoxide (H_2CO:CO = 1:1), formaldehyde and methane (H_2CO:CH_4 = 1:1), formaldehyde and methanol (H_2CO:CH_3OH = 1:1). Maintaining a constant temperature of 20 K and irradiating all samples with 1 MeV protons and analyzed with infrared spectroscopy before, during, and after irradiation. Although I was a part of all the different experiments, I will only comment on the results acquired from the pure formaldehyde experiment. The results of the experiment show that the irradiation of H_2CO prompts formation of complex molecules – including methanol, methyl formate and its isomer glycolaldehyde – together with simpler molecules such as carbon monoxide, carbon dioxide and methane.

Deposition vs. Irradiation

From Figure (4.1) it is clear that the characteristic molecular vibrational modes for H_2CO, such as the CO stretching mode and CH_2 scissoring mode, gets destroyed and creates other molecules – predominantly CO_2 at 2343 cm^{-1} and CO at 2139 cm^{-1} along with the characteristic broad band from water and methanol symmetric and asymmetric O-H stretching modes above 3000 cm^{-1}. It is also worth noting the formation of methane at 1302 cm^{-1} from formaldehyde *via* the irradiation following the reaction scheme

$$H_2CO \xrightarrow{H} CH_3O \xrightarrow{H} CH_3OH \xrightarrow{CR} CH_3\bullet + \bullet OH \xrightarrow{H} CH_4 + \bullet OH. \tag{5.1}$$

It is interesting to note the formation of a broad band spanning from ~ 1300 – 750 cm^{-1}. In this broad band we suspect methyl formate to make an appearance, however the entire band clearly cannot be assigned only to a single molecule. Therefore, a further discussion of determining the molecular components of this broad band will take place later in this section.

Destruction and Formation

As Figure (4.1) only depicts a single irradiation spectrum, it is difficult to comment on the rate of which a molecule gets destroyed or formed through the process of ion irradiation. Therefore, specific molecules with a narrow and single component absorption band positions have been examined separately and will be discussed individually. From each IR spectrum acquired after irradiation, a gaussian curve have been fitted around the central absorption band for each of the molecules (H_2CO, CO, CO_2 and CH_4) and the area has been calculated and converted to column density using Equation (4.1). The ion fluence has been converted to a dose using Equation (4.2). This allows for a comparison between the destruction and formation of each of the molecules as the sample gets irradiated. It is important to note that the area calculation of methanol is different compared to the other molecules – however this will be properly discussed later.

Formaldehyde, H_2CO

CR-induced photons can dissociate H_2CO and CH_3OH, creating functional group radicals, such as CH_3, on or within an icy grain mantle [Simons et al., 2019]. At temperatures as low as 20 K or above, radical-radical recombination becomes as favorable as hydrogenation of radicals and therefore leads to the formation of COMs [Simons et al., 2019]. Knowing this we would expect a decrease in formaldehyde as it gets irradiated by 1 MeV ions at 20 K and this is also what the results from Figure (4.2a) depicts. The column density of H_2CO falls off quickly as it gets irradiated, but as the dose increases the destruction smoothens out and reaches a value of roughly 1.25×10^{18} molecules cm^{-2} indicating that the amount of formaldehyde has been reduced drastically.

Carbon monoxide, CO

Carbon monoxide is expected to be created through the process of photodissociation of formaldehyde leading to the formation of a formyl radical and a hydrogen atom as seen in Equation (2.2). Then through the process of dehydrogenation the formyl radical will lose a hydrogen atom and be left with carbon monoxide and a hydrogen atom

$$H_2CO \xrightarrow{CR} HCO\bullet + H \tag{5.2}$$

$$HCO\bullet \xrightarrow{CR} CO + H \tag{5.3}$$

From Figure (4.2b) we see a steep increase in the amount of CO at low doses indicating that CO gets formed early through the irradiation of formaldehyde. However, as the dose increases the rate at which CO gets formed decreases but does not reach a plateau and thus continues to be formed.

Carbon dioxide, CO_2

Carbon dioxide follows a similar reaction scheme as the aforementioned carbon monoxide. However, carbon dioxide consists of one more oxygen atom. This leads to the formation of carbon dioxide to be slower than the formation of carbon monoxide which is also what the results in Figure (4.2c) shows. Compared to carbon monoxide in Figure (4.2b) the formation of CO_2 at sub 1 eV/16u doses is about 1 to 2 orders of magnitudes lower than that of CO. However, at doses 4 eV/16u to 15 eV/16u the formation of CO_2 seems to be efficient before reaching a plateau at higher doses.

Methane, CH_4

From Equation (5.1) it can be seen that one of the products through hydrogenation and photodissociation will eventually lead to the formation of methane along with a hydroxyl radical. However, as this is a rather complex reaction, it is expected that the formation of methane will be less efficient compared to the more abundant molecules such as CO, CO_2 and CH_3OH.

Indeed, from Figure (4.2d) it can be seen that the column density is of the order of 10^{16} molecules cm^{-2} which is orders of magnitudes lower than CO, CO_2 and CH_3OH. It can also be seen from the figure, that the peak arises at roughly 35 eV/16u which is way later than CH_3OH indicating that CH_4 might be a 2^{nd} generation molecule.

Methanol, CH_3OH

Since methanol happens earlier in the reaction scheme in Equation (5.1), it was interesting to examine the formation of methanol as well. However, since methanol's central absorption band lies within the broad band shown in Figure (4.3a), it was more challenging to calculate the area as it could have contributions from multiple molecules. I have identified a peak (peak 7 in Figure (4.3d)), which I have assumed only consists of methanol. Naturally, this infers a greater degree of uncertainty but still allow for the general behavioral trend to be examined. A further discussion of the molecular compent determination of the broad band follows after this section.

As the formation of methanol occurs before the formation of methane, it could be expected that methanol will have a higher abundance and gets formed at lower doses. Figure (4.2e) supports this claim as the column density is indeed greater than methane and the formation of methanol happens rapidly at low doses, however it clearly falls off quickly as well. This indicated that methanol gets formed early through hydrogenation however gets destroyed quickly *via* irradiation.

Determination of Broad Band

From Figure (4.1) an unlabled broad band appears in the range 1300 – 750 cm^{-1}. Trying to disentangle this band into each of the molecular components proved to be difficult. Therefore, three different methods of determining components will be discussed – a linear fit, pure ice summation and lastly a gaussian method.

The linear fitting can be seen in Figure (4.3b) where the area of each peak in the broad band has been calculated *via* a straight line from shoulder to shoulder. This way of fitting is not preferred as it cuts off way too much of contributions from multiple molecules. Since this way of fitting and determining molecules only examines a single peak individually from shoulder to shoulder, it does not take into account eventual contributions close to the integration limits.

A sligthly better way to fit the broad band is to consider what molecules could form in the sample and then add pure ice spectra for the chosen molecules. This method can be seen in Figure (4.3c) where multiple pure ice spectra have been added. It is important to note that the spectra does not depict absorbances but only the actual irradiation spectrum (solid black line) shows the correct absorbance. Each of the molecules' spectra have been scaled to allow for better determination of their central band positions. When adding all of the pure ice spectra together, a fit resembling the actual spectrum should occur, showcasing that the sample actually consists of the chosen molecules. See Figure (4.3a). However, this might be possible when fitting to a single component / narrow band, but when dealing with a broad band, as in this case, this fitting method also becomes unfavourable as there is no way to tell the abundances, temperatures, mixtures *et cetera* with this method and therefore also poses a substantial error and uncertainty. Although this method might not seem particularly useful, it can be used to figure out central band positions for the added ices and thus help determine the components in the original spectrum.

The final and preferred method can be seen in Figure (4.3d) where each of the identified peaks have been attributed their own gaussian fit. This method solves the problem of cutting off contributions that arised using linear fitting and builds on the strengths of the pure ice summation method. From the pure ice spectra I have identified a peak which seems to be solely affected by the abundance of methanol (Peak 7) in Figure (4.3d). Therefore, by assuming a symmetrical shape and singular contribution, I have been able to fit a gaussian and calculate the area used for the column density calculations *via* Equation (4.1). Doing this for all of the irradiation spectra I have produced Figure (4.2e) discussed in the previous section.

6 Conclusion

In this project, I have examined the formation of methyl formate and its isomers by conducting astrochemical experiments on site at the Ice Chamber for Astrophysics-Astrochemistry (ICA) facility at the Institute for Nuclear Research (Atomki) in Debrecen, Hungary. I Section (2), I described the characteristics of interstellar surface chemistry and briefly explained the theoretical background for some of the methods used in Section (3).

My results, presented in Section (4), suggest that the process of 1 MeV H^+ ion irradiation at 20 K of formaldehyde, H_2CO, destroys the molecule and prompts the formation of carbon monoxide (CO), carbon dioxide (CO_2), methane (CH_4) and methanol (CH_3OH).

Examining the formation of methyl formate and its isomers proved more difficult than initally anticipated as the central absorption band for methyl formate was located within a broad band spanning hundreds of wavenumbers. Therefore, an analysis of the best way of fitting to molecules was carried out. These methods include a disfavored linear fitting, a slightly better summation of pure ice spectra, and finally a preferred gaussian fitting along with the summation method.

Bibliography

Arumainayagam, C. R., Garrod, R. T., Boyer, M. C., Hay, A. K., Bao, S. T., Campbell, J. S., Wang, J., Nowak, C. M., Arumainayagam, M. R., and Hodge, P. J. (2019). *Extraterrestrial prebiotic molecules: Photochemistry vs. radiation chemistry of interstellar ices. Chemical Society Reviews*, 48(8):2293–2314.

Bacmann, A., Taquet, V., Faure, A., Kahane, C., and Caccarelli, C. (2012). *Detection of complex organic molecules in a prestellar core: a new challenge for astrochemical models. Astronomy and Astrophysics*, 541, May 2012(L12):5.

Bouilloud, M., Fray, N., Bénilan, Y., Cottin, H., Gazeau, M. C., and Jolly, A. (2015). *Bibliographic review and new measurements of the infrared band strengths of pure molecules at 25 K: H2O, CO2, CO, CH4, NH3, CH3OH, HCOOH and H2CO. Monthly Notices of the Royal Astronomical Society*, 451(2):2145–2160.

Burton, M., Crocker, R., Dickey, J., Filipovic, M., Purcell, C., Rathborne, J., Rowell, G., Tothill, N., and Walsh, A. (2013). *The Interstellar Medium White Paper. arXiv e-prints*, page arXiv:1307.0712.

Herbst, E. (1995). *Chemistry in the Interstellar Medium. Annual Review of Physical Chemistry*, 46:27–54.

Herbst, E. and van Dishoeck, E. F. (2009). *Complex Interstellar Organic Molecules. Annual Review of Astronomy and Astrophysics*, 427, 2009(47):80.

Herczku, P., Mifsud, D. V., Ioppolo, S., Juhász, Z., Kaňuchová, Z., Kovács, S. T. S., Traspas Muiña, A., Hailey, P. A., Rajta, I., Vajda, I., Mason, N. J., McCullough, R. W., Paripás, B., and Sulik, B. (2021). *The Ice Chamber for Astrophysics–Astrochemistry (ICA): A new experimental facility for ion impact studies of astrophysical ice analogs. Review of Scientific Instruments*, 92(8):084501.

Ioppolo, S., Fedoseev, G., Chuang, K.-J., Cuppen, H. M., Clements, A. R., J. M., Garrod, R. T., Qasim, D., Kofman, V., van Dishoeck, E. F., and Linnartz, H. (2021). *A non-energetic mechanism for glycine formation in the interstellar medium. Nature Astronomy*, 5, February 2021(2):197–205.

Ioppolo, S., van Boheemen, Y., Cuppen, H. M., van Dishoeck, E. F., and Linnartz, H. (2011). *Surface formation of CO2 ice at low temperatures. Monthly Notices of the Royal Astronomical Society*, 413, May 2011(3):2281–2287.

Linnartz, H., Ioppolo, S., and Fedoseev, G. (2015). *Atom addition reactions in interstellar ice analogues. International Reviews in Physical Chemistry*, 34(2):205–237.

Mifsud, D. V., Herczku, P., Rácz, R., Rahul, K. K., Kovács, S. T. S., Juhász, Z., Sulik, B., Biri, S., McCullough, R. W., Kaňuchová, Z., Ioppolo, S., Hailey, P. A., and Mason, N. J. (2022). *Energetic electron irradiations of amorphous and crystalline sulphur-bearing astrochemical ices. Frontiers in Chemistry*, 10.

Mifsud, D. V., Juhász, Z., Herczku, P., Kovács, S. T. S., Ioppolo, S., Kaňuchová, Z., Czentye, M., Hailey, P. A., Muiña, A. T., Mason, N. J., McCullough, R. W., Paripás, B., and Sulik, B. (2021). *Electron irradiation and thermal chemistry studies of interstellar and planetary ice analogues at the ICA astrochemistry facility. The European Physical Journal D*, 75(6):182.

Osterbrock, D. (1984). *Introduction to the Interstellar Medium.* Author's UCSC course notes, University of California, Santa Cruz, The United States of America.

Pontoppidan, K. M. (2006). *A direct measurement of CO depletion and the formation of CO_2. Astronomy and Astrophysics*, 453, July 2006(3):L47–L50.

Ryden, B. and Peterson, B. M. (2021). *Foundations of Astrophysics.* Cambridge University Press, Cambridge, United Kingdom.

Simons, M. A. J., Lamberts, T., and Cuppen, H. M. (2019). *Formation of COMs through CO hydrogenation on interstellar grains. Astronomy and Astrophysics*, 634, February 2020(A52):13.

Tielens, A. G. G. M. (2021). *Molecular Astrophysics.* Cambridge University Press, Cambridge, United Kingdom.

Whittet, D. C. B., Poteet, C. A., Chiar, J. E., Pagani, L., Bajaj, V. M., Horne, D., Shenoy, S. S., and Adamson, A. J. (2013). *ICE AND DUST IN THE PRESTELLAR DARK CLOUD LYNDS 183: PREPLANETARY MATTER AT*

THE LOWEST TEMPERATURES. The Astrophysics Journal, 744, August 2013(2):15.

Williams, D. A. and Herbst, E. (2002). *It's a dusty Universe: surface science in space. Surface Science*, 500(1):823–837.

Ziegler, J. F., Ziegler, M., and Biersack, J. P. (2010). *SRIM – The stopping and range of ions in matter (2010). Nuclear Instruments & Methods in Physics Research Section B-beam Interactions With Materials and Atoms*, 268:1818–1823.

A SRIM Stopping Power Simulations

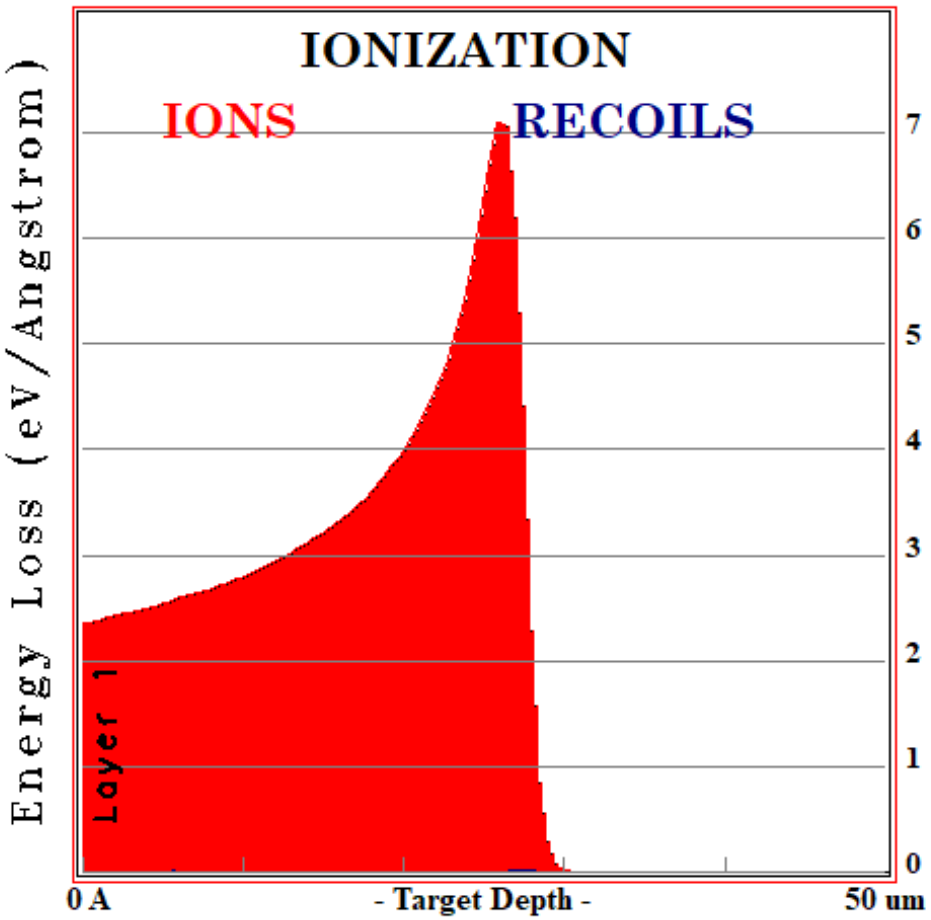

Figure A.1: SRIM simulations of formaldehyde H_2CO being irradiated with 1 MeV H^+ ions. The Bragg peak is clearly visible depicting the maximum loss of energy before the ions come to rest. Figure kindly obtained by Zuzana Kaňuchová from Slovak Academy of Sciences.

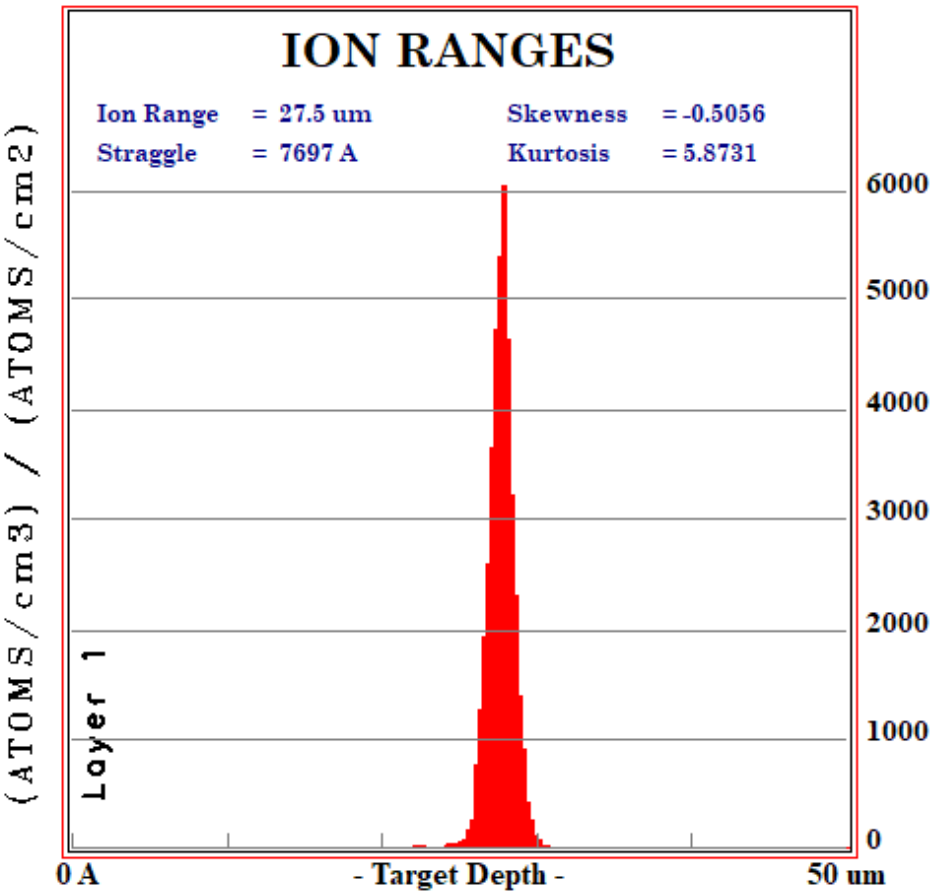

Figure A.2: SRIM simulations of formaldehyde H_2CO being irradiated with 1 MeV H^+ ions. Depicts the ion range. Figure kindly obtained by Zuzana Kaňuchová from Slovak Academy of Sciences.

B Deposition vs. Irradiation

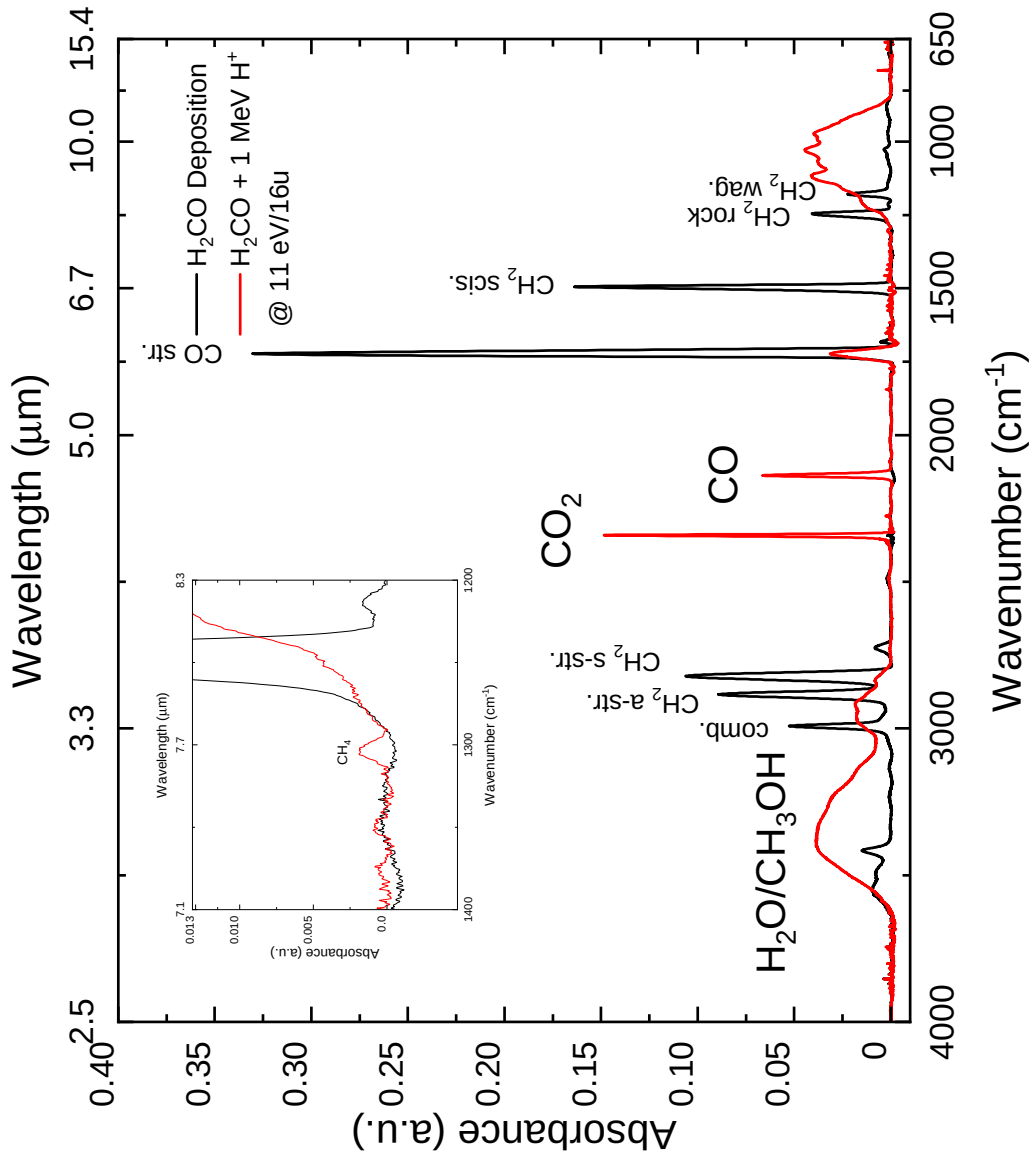

Figure B.1: FTIR spectrum of pure H_2CO deposition (solid black line) together with FTIR spectrum of the ice irradiated by 1 MeV energetic ions at 20 K (solid red line). Additionally, each of the characteristic modes for H_2CO have been labeled together with the absorption peaks for CO, CO_2 and CH_4 which are also the absorption bands used to calculate the area used in the calculation for column densities. Moreover, the characteristic broad band for water and methanol (CH_3OH) is also labeled. Figure discussed in Section (5).

C Destruction and Formation

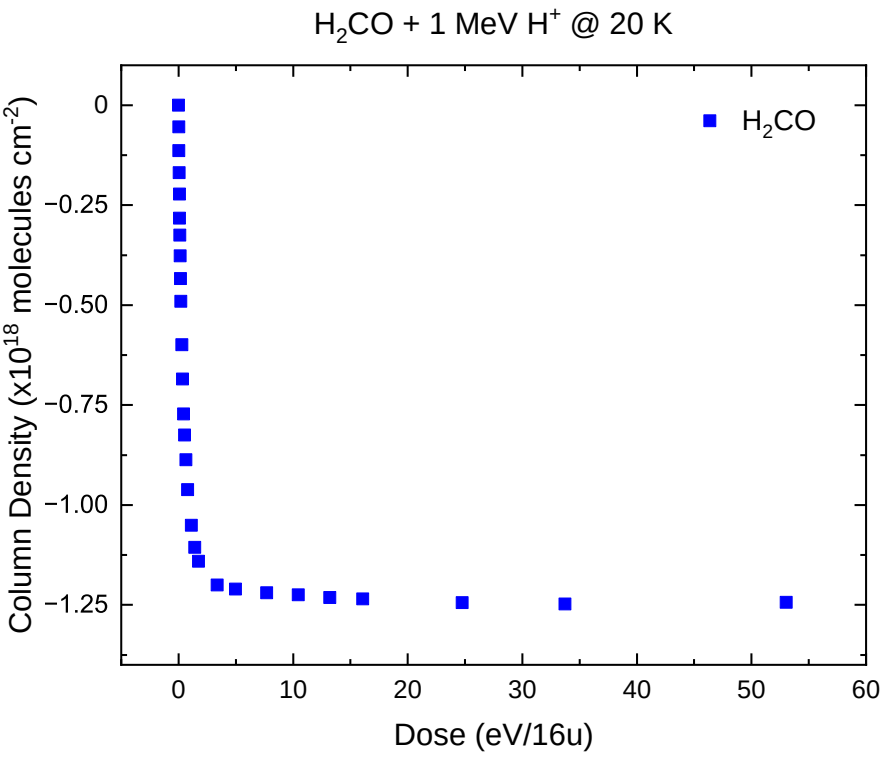

Figure C.1: Destruction of formaldehyde H_2CO due to irradiation of 1 MeV H^+ ions at 20 K.

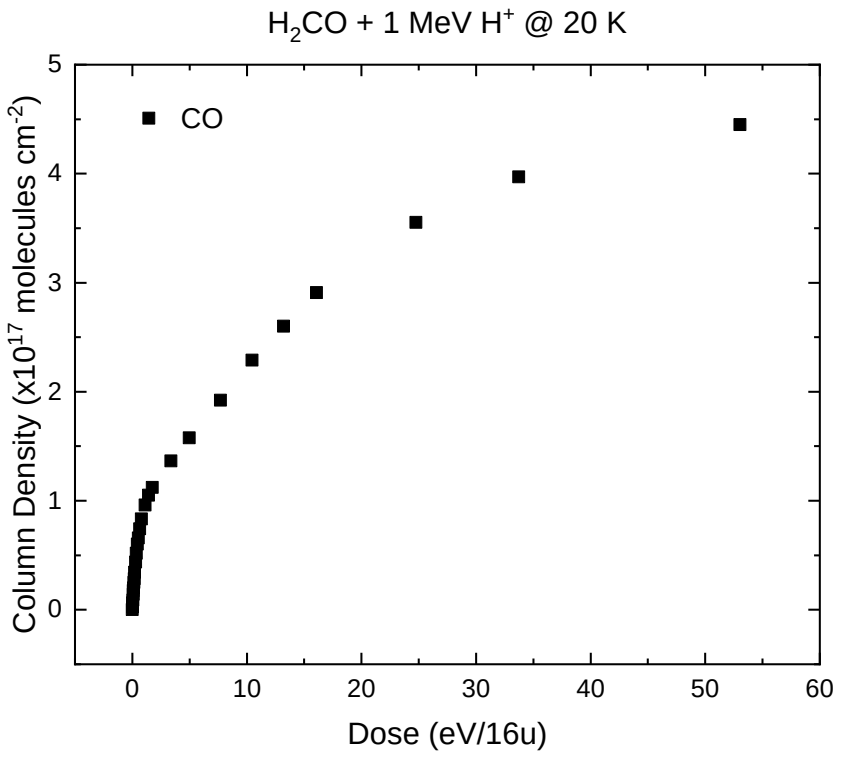

Figure C.2: Formation of carbon monoxide (CO) under 1 MeV H^+ ion irradiation of H_2CO at 20 K.

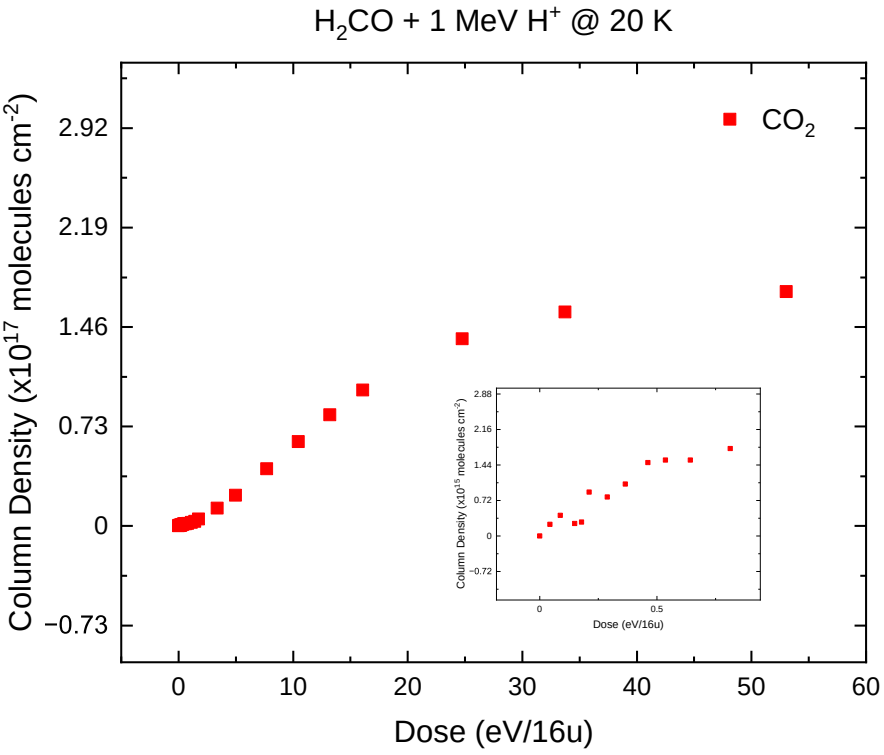

Figure C.3: Formation of carbon dioxide (CO_2) under 1 MeV H^+ ion irradiation of H_2CO at 20 K.

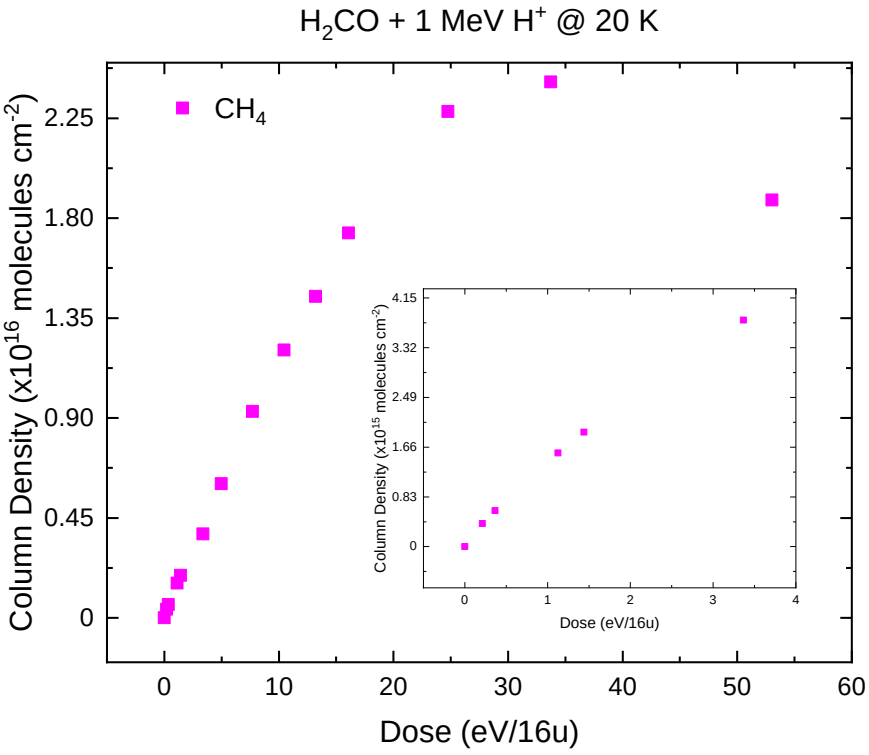

Figure C.4: Formation of methane (CH_4) under 1 MeV H^+ ion irradiation of H_2CO at 20 K.

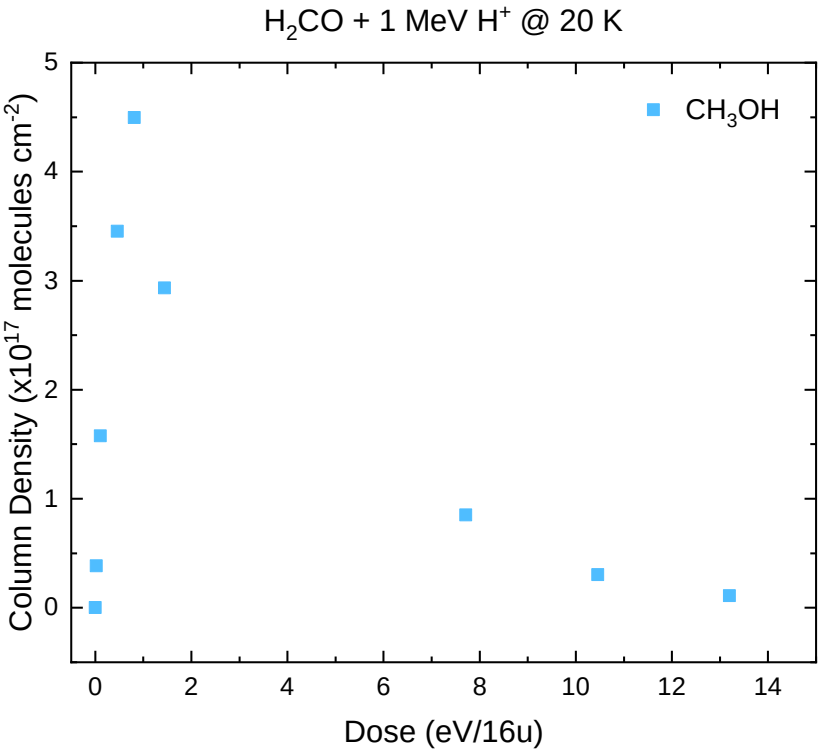

Figure C.5: Formation of methanol (CH_3OH) under 1 MeV H^+ ion irradiation of H_2CO at 20 K. Areas acquired by fitting a gaussian at Peak 7 in Figure (4.3b) or Figure (4.3d) which lies directly in the middle of a broad band. Therefore a substantial uncertainty is followed in the column density however the general behavioral trend is trustworthy.

D Determination of Broad Band

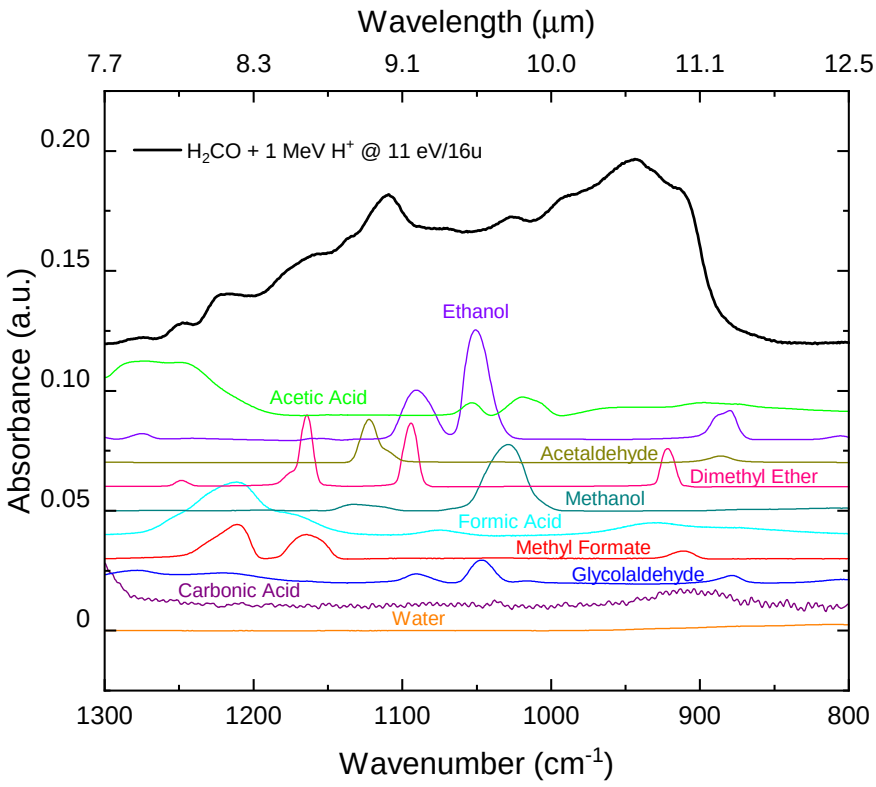

Figure D.1: Labelling of all of the different pure ice components that could make up the observed spectrum of H_2CO irradiated with 1 MeV H^+ ions at 20 K at the dose 11 eV/16u.

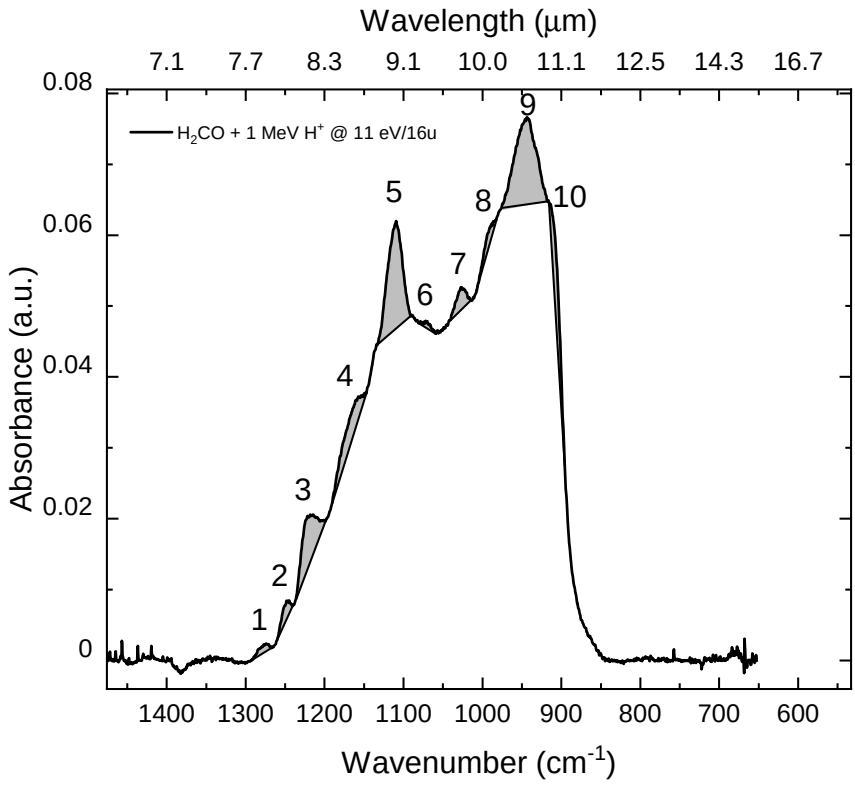

Figure D.2: One way of determining what the peaks in the broad band could consists of is using a linear way of intergration beneath the peaks. However, this way has some serious downsides as discussed in section (5).

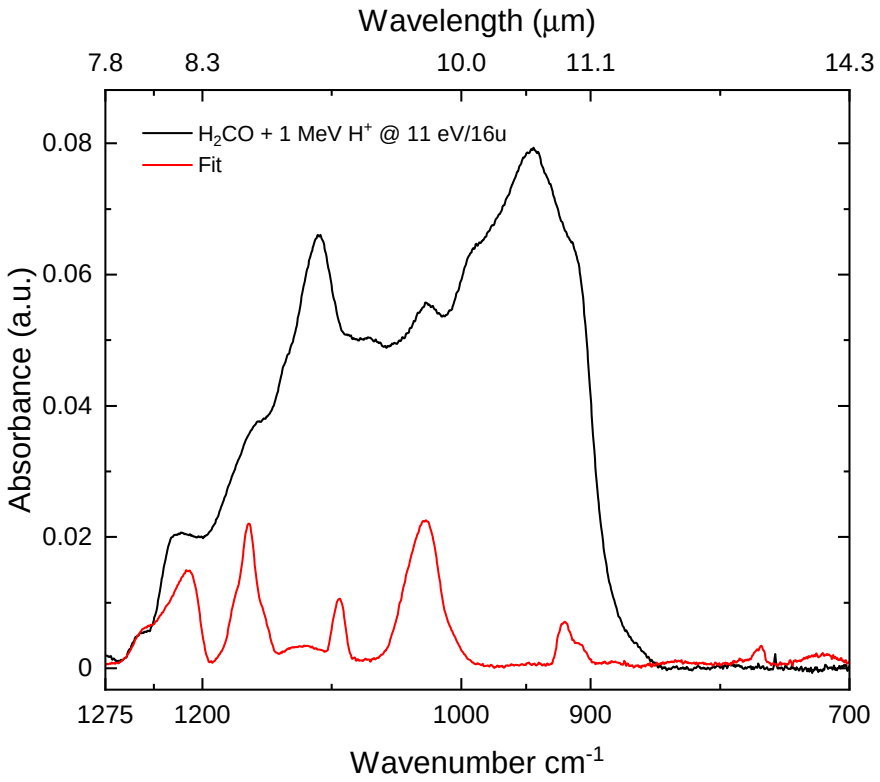

Figure D.3: Another way to determine the contributions of the individual pure species could be to sum each of their spectra and create a fit this way. The disadvantages of this method is discussed in section (5).

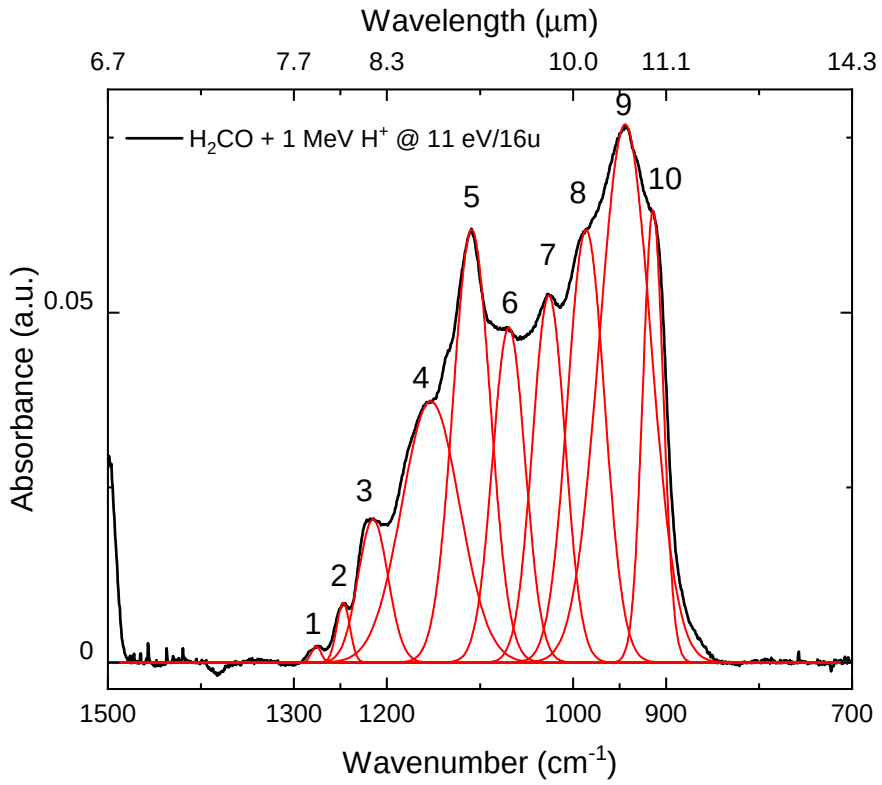

Figure D.4: The preferred way of disentangling a broad band is done by fitting a gaussian underneath each peak and then calculate the area in this region throughout each irradiation. This method is further discussed in section (5).

E Pictures From Atomki

Figure E.1: Group photo taken at the ICA facility.

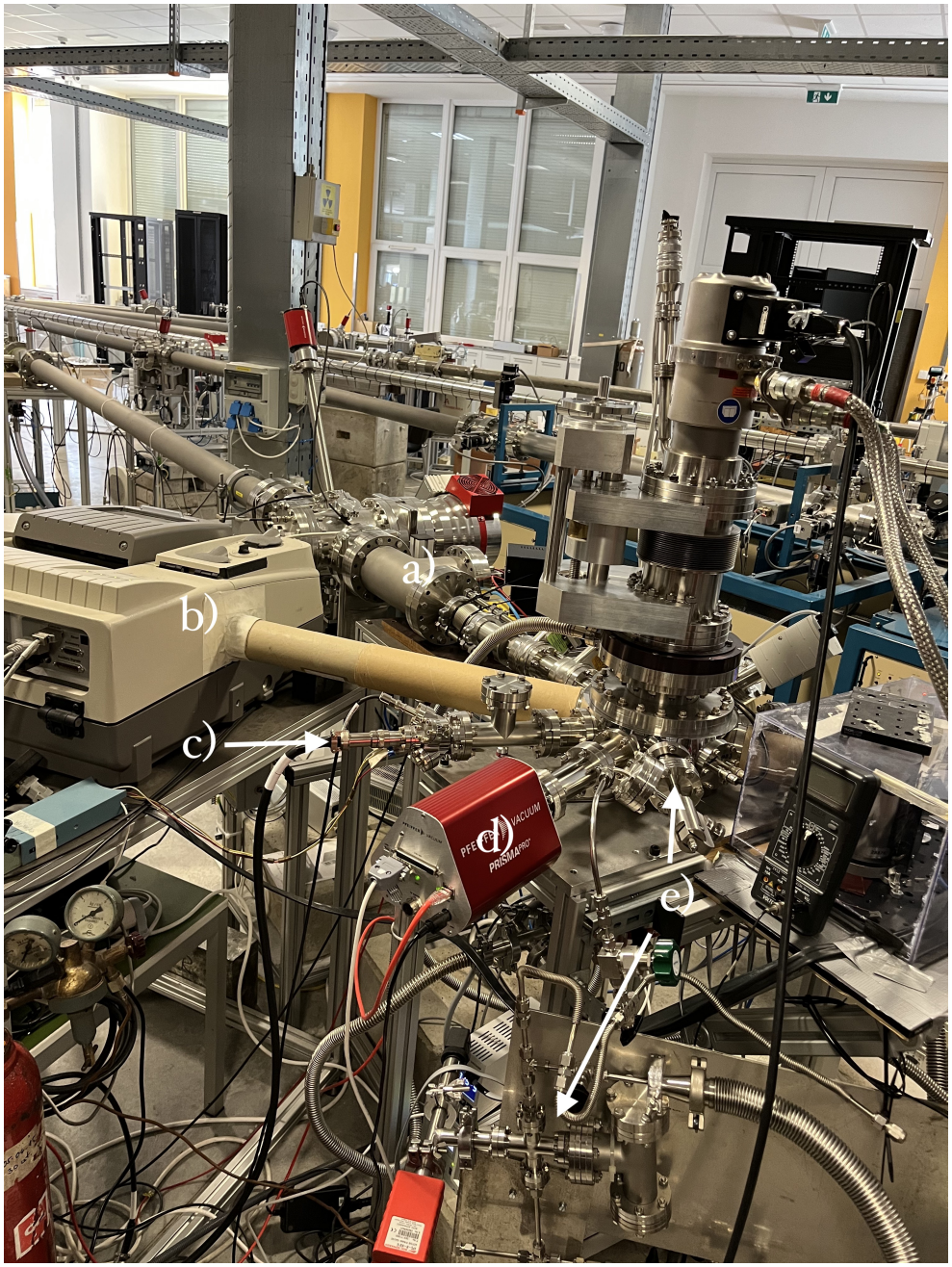

Figure E.2: The end station at the ICA facility. **a)** is the H^+ ion beam line. **b)** is the IR spectrograph and IR beam module. **c)** is the Kimball ELG-2A electron gun. **d)** Quadrupole mass spectrometer. **e)** being the gas inlet and mixing station allowing for background deposition.

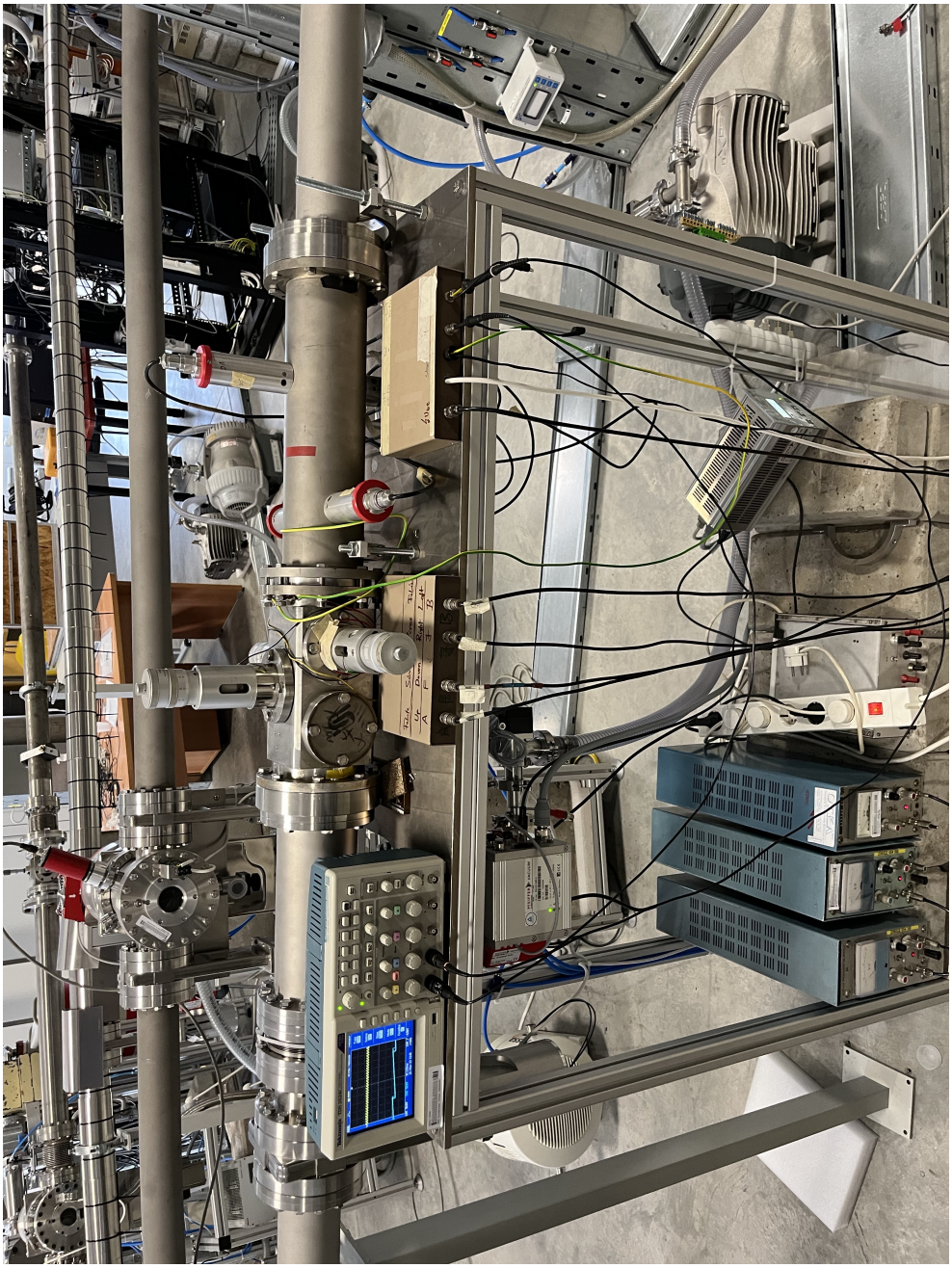

Figure E.3: Two sets of 4x4 electrode steerer plates, one vibrating perpendicular and one parallel to beam. Notice the screen on the left showing the perpendicular steerer plate vibrating at low frequency and the parallel steerer plate vibrating at high frequency.

Figure E.4: The ICA facility with its many "fingers" leading to individual end stations. The white arrow marks the end station used for the experiments.

Figure E.5: Deposition of formaldehyde (H_2CO) *via* direct deposition. Notice that formladehyde is a powder at room temperature.